Received: 23 June 2020 | Revised: 22 April 2021 | Accepted: 23 April 2021

DOI: 10.1002/kin.21503

INTERNATIONAL JOURNAL OF CHEMICAL KINETICS WILEY

RESEARCH ARTICLE

Observation of low-temperature chemistry products in laminar premixed low-pressure flames by molecular-beam mass spectrometry

Thomas Bierkandt[1] | **Patrick Oßwald**[1] | **Nina Gaiser**[1] | **Dominik Krüger**[1] | **Markus Köhler**[1] | **Martin Hoener**[2] | **Shkelqim Shaqiri**[2] | **Dennis Kaczmarek**[2] | **Yasin Karakaya**[2] | **Patrick Hemberger**[3] | **Tina Kasper**[2]

[1] German Aerospace Center (DLR), Institute of Combustion Technology, Stuttgart, Germany

[2] Mass Spectrometry in Reactive Flows, University of Duisburg-Essen, Duisburg, Germany

[3] Laboratory for Synchrotron Radiation and Femtochemistry, Paul Scherrer Institute, Villigen, Switzerland

Correspondence
Thomas Bierkandt, Institute of Combustion Technology, German Aerospace Center (DLR), Stuttgart 70569, Germany.
Email: thomas.bierkandt@dlr.de

Funding information
European Community's Seventh Framework Program (FP7/2007-2013), Grant/Award Number: 312284; German Research Foundation, Grant/Award Numbers: KA3871/3-2, KO4786/2-2; Swiss Federal Office of Energy, Grant/Award Number: SI/501269-01

Abstract

The formation of typical low-temperature oxidation products is observed in laminar premixed low-pressure flames investigated by photoionization molecular-beam mass spectrometry at the Swiss Light Source. The C_1–C_4 alkyl hydroperoxides can be identified in *n*-butane- and 2-butene-doped hydrogen flames by their photoionization efficiency spectra at *m/z* 48, 62, 76, and 90. C_1–C_3 alkyl hydroperoxides are also observed in a propane-doped hydrogen flame and in a neat propane flame. In addition, threshold photoelectron spectra reveal the presence of the alkyl hydroperoxides. In the 2-butene/H_2 flame, the photoionization spectrum at *m/z* 88 also enables the identification of butenyl hydroperoxides by comparison with calculated ionization energies of the alkenyl hydroperoxides and a literature spectrum. The low-temperature species are formed close to the burner surface with maximum mole fractions at 0.25–0.75 mm above the burner. At 0.5 mm, even the methylperoxy radical (CH_3OO) is measured for the first time in a laminar premixed flame. The rate of production analyses show that consumption of the hydroperoxyalkyl radicals results in the formation of cyclic ethers. In the *n*-butane/H_2 flame, ethylene oxide, oxetane, and methyloxirane are identified. Besides expected small oxygenated species, for example, formaldehyde or acetaldehyde, the larger C_4 oxygenates butanone ($C_2H_5COCH_3$) and 2,3-butanedione ($C_4H_6O_2$) are formed in the two C_4 hydrocarbon-doped hydrogen flames. Quantification of alkyl hydroperoxides with estimated photoionization cross sections based on the corresponding alcohols, which have similar photoelectron structures to the alkyl hydroperoxides, shows that mole fractions are on the order of 10^{-5}–10^{-6} in the *n*-butane/H_2 flame. Measurements are corroborated by simulations, which also predict the presence of some peroxides in detectable concentrations, that is, mole fractions larger than 10^{-7}, under the investigated

conditions. The observation of peroxide species and cyclic ethers in the investigated laminar premixed flames give new insights into the contribution of low-temperature combustion chemistry in a flame.

KEYWORDS
flame-sampling molecular-beam mass spectrometry, hydroperoxides, low-temperature oxidation, photoelectron photoion coincidence spectroscopy, photoionization

1 | INTRODUCTION

Advanced combustion strategies and novel fuels are a key factor in future energy supply and transportation as they promise improved efficiencies and reductions of carbon dioxide and air pollutant emissions. Fuel composition also plays a crucial role in the exhaust emissions from internal combustion in engines[1,2] or gas turbines.[3,4] A particular focus of engine development is the use of combustion processes at low temperatures.[5,6] The low-temperature combustion (LTC) can have a positive impact on the trade-off between nitrogen oxides (NO_x) and soot.[6–8] LTC is implemented in various forms, for example, as homogeneous charge compression ignition (HCCI) or reactivity controlled compression ignition (RCCI).[6,9] In all of these processes, a homogeneous mixture of fuel and air is autoignited by compression. To control these processes, understanding the ignition and oxidation properties of various fuels is essential but challenging.[10] The typical LTC regime is located between 450 and 850 K[11] and a reaction sequence for the low-temperature oxidation of an alkane (RH) is shown in Figure 1. The LTC is especially relevant for cool flames and low-temperature ignition in automotive engines.

Fuel consumption is mostly initiated by OH radicals to produce the corresponding alkyl radicals (R), for example, 1-butyl and 2-butyl radicals (C_4H_9) in the oxidation of *n*-butane (C_4H_{10}). This is also the main initiation step for the fuel consumption in the high-temperature combustion, for example, in a laminar premixed flame. In such a flame environment, a β-scission follows the initiation step of fuel decay, while the alkyl radicals react with molecular oxygen (O_2) in the low-temperature regime to alkylperoxy radicals (ROO) as presented in Figure 1. Further reactions of the ROO radical lead to the formation of alkyl hydroperoxides (ROOH), alkenes, or hydroperoxyalkyl radicals (QOOH). The hydroperoxyalkyl radical is formed by isomerization via internal H-abstraction.[13] Consumption pathways of the QOOH radical into cyclic ethers, aldehydes, or ketones and reaction to alkenyl hydroperoxides by β-scission contribute to the negative temperature coefficient behavior,[11] while a second O_2 addition to the QOOH radical can result into the formation of hydroperoxyalkylperoxy radicals (OOQOOH). Further branching agents of the OOQOOH radical may be ketohydroperoxides, alkenyl hydroperoxides, or diones. The isomerization of the OOQOOH radical also opens the pathway for a third O_2 addition. For example, Wang et al. detected highly oxygenated species formed by a third O_2 addition during the oxidation of 2,5-dimethylhexane[14] and *n*-heptane.[15] The fate of the OOQOOH radical during *n*-pentane oxidation in a jet-stirred reactor towards ketohydroperoxides and their further decomposition to carboxylic acids was recently studied by electron-ion coincidence mass spectrometry.[16]

The alkylperoxy radical can react with the hydroperoxyl radical (HO_2), the smallest peroxide, to form an alkyl hydroperoxide (ROOH) as shown in Figure 1 and mentioned above. DeCorpo et al. quantified the methyl hydroperoxide (CH_3OOH) in 1973 by mass spectrometry in a cool acetaldehyde flame, which was stabilized in a flow reactor operated at atmospheric pressure.[17]

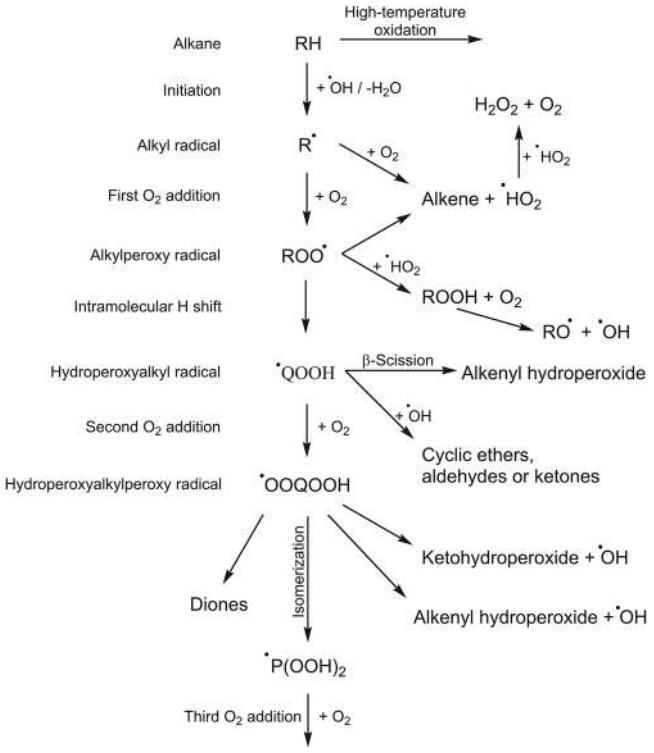

FIGURE 1 Scheme for the low-temperature oxidation of an alkane (after Wang et al.[12])

In another early study, Taylor identified some peroxide species, for example, hydrogen peroxide (H_2O_2) and *tert*-butyl hydroperoxide (C_4H_9OOH), by paper chromatography below and above the cool-flame limit of isobutane.[18] Hydroperoxides were intensely studied in the last 10 years during the low-temperature oxidation of alkanes in jet-stirred reactors. A current overview was given by Wang et al.,[12] while Herbinet et al.[19] summarized the period from 1990 to 2013. The reactors were often coupled to a time-of-flight mass spectrometer with photoionization to allow isomer-resolved in situ detection of the elusive peroxide species, but in some works also gas chromatography, FTIR spectroscopy, or infrared cavity ring-down spectroscopy were used as the analytical method to capture the low-temperature chemistry.[12] Detailed speciation data of hydroperoxides were measured for the first time by Battin-Leclerc et al. for the oxidation of *n*-butane between 560 and 720 K.[20] Methyl, ethyl, and butyl hydroperoxides were identified based on their ionization energies by photoionization efficiency (PIE) spectra in the photon energy range from 8.5 to 11.5 eV.[20,21] Further progress in the detection of low-temperature species and in understanding the LTC of hydrocarbons was reported for the oxidation of propane,[22,23] *n*-butane,[24–26] *n*-pentane,[27] *n*-heptane,[28] or 1-hexene.[29] Recently, Bourgalais et al.[30] coupled a jet-stirred reactor (JSR) for the first time to a double imaging photoelectron photoion coincidence (i^2PEPICO) spectrometer at the synchrotron SOLEIL to obtain threshold photoelectron (TPE) spectra for species generated upon low-temperature oxidation of *n*-pentane. They measured photoelectron spectra of the smallest alkyl hydroperoxides, that is, methyl and ethyl hydroperoxide, and were able to resolve isomers at mass-to-charge ratios of 72, 84, 86, and 88.[30]

In laminar premixed flames, the temperature rises rapidly from the preheat zone to the end of the reaction zone and hence high-temperature combustion is the dominant oxidation mechanism. However, low-temperature species from the scheme in Figure 1 may also be formed in the preheat zone of the flame close to the burner. Under some conditions, the flame temperature in this zone can be smaller than 850 K and thus trigger low-temperature oxidation. After leaving the preheat zone, low-temperature species will decompose quickly with rising temperature at the transition to intermediate (850–1200 K) and high-temperature oxidation (>1200 K). The dominant consumption pathway of alkyl hydroperoxides (ROOH) is the decomposition into alkoxy (RO) and OH radicals by dissociation of the oxygen–oxygen bond.[12] At intermediate temperatures, the small peroxide species H_2O_2 contributes to chain branching by decomposing into two OH radicals.[31] Hydrogen peroxide (H_2O_2) itself is stable up to 1100 K and is formed by H-abstraction reactions of HO_2.[13] The first reliable quantification of H_2O_2 formed during LTC was presented by Bahrini et al. for the oxidation of *n*-butane.[32]

Experimental detection of alkyl hydroperoxides in flame-sampling experiments was recently reported by Zhang et al. for ethylene, ethane, propene, and *n*-butane laminar premixed, low-pressure flames.[33] Kinetic modeling of flames with a reaction mechanism that has included low-temperature chemistry and probe-perturbed temperature profiles have shown that these elusive species may be formed closer to the burner,[33] where the flame temperatures are generally lower. Zhang et al. also showed for an ethylene flame that model results can be significantly improved by using the probe-disturbed temperature profile. They concluded that formation of low-temperature species in the preheat zone of their investigated flames originated from the temperature reduction by the sampling probe perturbation.[33] However, concentrations of only some low-temperature related combustion intermediates, for example, ethanol, were affected, while the formation of typical high-temperature combustion intermediates from the reaction zone was not influenced.[33]

We report about the formation of alkyl hydroperoxides, the methylperoxy radical, and cyclic ethers in alkane- (*n*-butane and propane) and alkene-doped (2-butene) hydrogen flames and in a neat propane flame. Species were identified by their PIE and TPE spectra measured by photoelectron photoion coincidence (PEPICO) spectroscopy. For the *n*-butane/H_2 flame, all detected species were quantified so that a comprehensive dataset including low-temperature species is available.

2 | EXPERIMENT

2.1 | Investigated flames

Fuel-rich, laminar premixed hydrogen flames doped with *n*-butane (*n*-C_4H_{10}), *trans*-2-butene (2-C_4H_8), and propane (C_3H_8) and a neat propane flame at the same equivalence ratio (Φ) of 1.25 were investigated at the vacuum ultraviolet (VUV) beamline of the Swiss Light Source. The flames were stabilized on a flat flame burner at 40 mbar and diluted with argon. Argon dilution was 25% and 50% for the hydrocarbon-doped hydrogen flames and the neat propane flame, respectively. Argon (99.998%), O_2 (99.998%), H_2 (99.995%), and propane (99.5%) were delivered by Carbagas, *n*-butane (99.95%) by Air Liquide, and *trans*-2-butene (99.5%) by Linde. To allow for comparable conditions, the three hydrocarbon-doped hydrogen flames had the same C, H, and O flow as used in a previous work.[34] The exact gas flows are summarized in Table 1.

Flame gases were sampled by molecular-beam technique and analyzed by PEPICO spectroscopy as described

TABLE 1 Flame conditions of the hydrocarbon-doped hydrogen flames and the neat propane flame

Flame	Φ	d_{Burner} (mm)	p (mbar)	$v_{298\,K}$ (cm/s)	$\dot{V}_{Hydrocarbon}$ (sccm)	$\dot{V}_{H_2}$ (sccm)	$\dot{V}_{O_2}$ (sccm)	$\dot{V}_{Ar}$ (sccm)
n-C_4H_{10}/H_2	1.25	60	40	65.20	100	1700	1200	1000
2-C_4H_8/H_2	1.25	60	40	66.83	100	1800	1200	1000
C_3H_8/H_2	1.25	60	40	65.20	133	1667	1200	1000
C_3H_8	1.25	60	40	65.20	400	0	1600	2000

in detail in the Supporting Information. Except for the n-butane/H_2 flame, the i^{2}PEPICO setup[35,36] was used for the investigation of the flames. The i^{2}PEPICO setup is also described by Sztáray et al.[36] and Hoener et al.[37] for photolysis and pyrolysis experiments to study reaction kinetics and a new high-pressure reactor experiment, respectively. A schematic sketch of this setup is shown in Figure S1 in the Supporting Information. The n-butane-doped hydrogen flame was measured with the single-imaging photoelectron photoion coincidence (iPEPICO) setup as described by Oßwald et al.[38] for flame-sampling molecular-beam mass spectrometry. The difference between these two setups is that the photoions are also velocity map imaged with the i^{2}PEPICO spectrometer.

Several burner scans, where the photon energies remain constant and the burner positions are varied between 0.25 and 30.25 mm with respect to the sampling probe, were performed in the n-butane/H_2 flame for photon energies of 7.59, 8.5, 9.15, 9.4, 9.7, 10.02, 10.36, 11.5, 12.3, 13.02, 13.7, 14.35, and 16.2 eV. Photon energies are selected to allow for a comprehensive separation of isomers. This flame is part of a series of alkane- and alkene-doped hydrogen flames designed to systematically study the hydrogen abstraction and fuel radical formation.[34] The mole fraction profiles of the 1-butyl and 2-butyl radicals and the major species that are most relevant for the discussion of fuel radical formation and branching ratios were presented previously by Krüger et al.[34] Here, we provide the experimental mole fraction dataset for more than 30 combustion species of the n-butane/H_2 flame within the Supporting Information and focus on the identification and formation of low-temperature species in the following discussion. The large number of photon energies used for the burner scans helps to determine mole fractions of most intermediates at photon energies close to their ionization energies. Burner scans in the n-butane/H_2 flame were performed from 0.25 to 4.25 mm with a step size of 0.25 mm, from 4.25 to 7.25 mm with 0.5 mm steps, from 7.25 to 12.25 mm with 1 mm steps, and from 12.25 to 30.25 mm with 2 mm steps. Energy scans at a fixed height above the burner (HAB) and different photon energies were performed in the preheat zone at HAB of 0.5 and 0.75 mm in the hydrocarbon-doped hydrogen flames and the neat propane flame, respectively. The photon energies were typically between 9 and 11.5 eV for identification of the alkyl hydroperoxides and other combustion intermediates by their PIE or photoelectron spectra. The scan resolution was 25 meV for all energy scans. The photon energy was calibrated by measuring the autoionization states of argon (11s′–13s′) between 15.75 and 15.83 eV in both the first and second order. The procedure for calculation of the mole fraction profiles is described in detail by Oßwald et al. for the flame-sampling setup at the VUV beamline of the Swiss Light Source.[38] Uncertainty of the experimental mole fractions is estimated to be 15–20% for the main species and 30–50% for the intermediate combustion species with known photoionization cross sections. For species with unknown photoionization cross section, the mole fraction uncertainties of a factor of 2–4 can be expected.[39] Overall uncertainties in flame-sampling molecular-beam mass spectrometry were discussed by Egolfopoulos et al.[40]

2.2 | Modeling of the n-butane-doped hydrogen flame

The AramcoMech 2.0 [Ref. 41] by the Combustion Chemistry Centre at NUI Galway was used without modifications for modeling of combustion species mole fraction profiles in the n-butane/H_2 flame. This mechanism builds upon the AramcoMech 1.3 [Ref. 42] and contains low-temperature and high-temperature chemistry for hydrogen, C_1–C_4 hydrocarbons and some oxygenated fuels. It was well validated against numerous experiments including flames, jet-stirred reactors, and shock tubes and therefore covers a wide range of different combustion parameters reliably. It was shown by Jithin et al.[43] that the AramcoMech 2.0 provides good agreement to capture the effect of hydrogen addition in the laminar burning velocity of n-butane/air flames. For autoignition, Jiang et al.[44] and Lee and Song[45] showed that the AramcoMech 2.0 is also able to predict ignition delay times of hydrogen/n-butane mixtures measured in a shock tube and with a rapid compression machine, respectively. It is expected that this model performs well for the investigation of the low-temperature chemistry in our n-butane-doped hydrogen flame.

We used the Cantera flame reactor module for burner-stabilized flames within the Chemical Workbech[46]

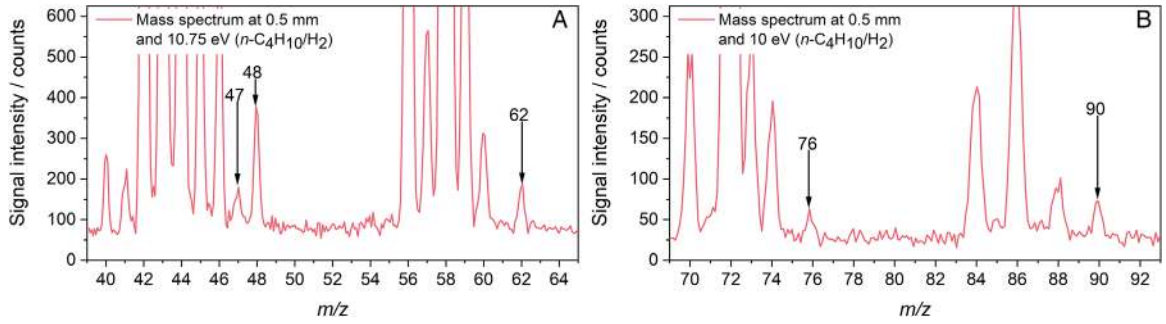

FIGURE 2 (A) Mass spectra at 10.75 and (B) 10 eV obtained for the *n*-butane/H_2 flame at a distance of 0.5 mm from the burner surface

(Kintech Lab) for the chemical kinetics simulation with the AramcoMech 2.0. The multicomponent transport model considering thermodiffusion was used. The experimentally determined temperature profile reported by Krüger et al.[34] for the *n*-butane/H_2 flame was used as input for the simulation. The exhaust gas temperature of the *n*-butane-doped hydrogen flame was measured by a coated thermocouple, and the temperature profile was then determined from the temperature dependence of the gas flow through the sampling nozzle to obtain a probe-perturbed temperature profile.[34] The experimental mole fraction profiles of the major species were well predicted by the ArmacoMech 2.0 using this temperature profile as shown by Krüger et al.[34]

3 | RESULTS AND DISCUSSION

The focus of this study is on the identification of some low-temperature species for a series of hydrocarbon-doped hydrogen flames and in a neat propane flame investigated by molecular-beam mass spectrometry. PIE and TPE spectra are used in the following to identify low-temperature species. At *m/z* 47, 48, 62, 76, and 90, the methylperoxy radical and alkyl hydroperoxides have been identified. Furthermore, the isomer composition of other oxygenates at *m/z* 44, 58, and 72 are explored. For the *n*-butane/H_2 flame, only PIE spectra of the low-temperature species can be presented, because the signal intensity was too low to obtain high-quality TPE spectra. For the other flames, averaging times were increased to successfully record TPE spectra of low-temperature species. These are presented here. For the sake of brevity, not all measured spectra from the four flames are shown. Identification is accompanied by the interpretation of possible reaction pathways obtained from AramcoMech 2.0.[41] This mechanism is suitable for reproducing the mole fractions of many stable C_1-C_4 combustion intermediates measured in the *n*-butane/H_2 flame (see Figure S2 and discussion in the Supporting Information). The further focus is therefore on quantification of alkyl hydroperoxides and other oxygenated combustion intermediates to provide more insights into their combustion kinetics. For example, the formation of 2,3-butanedione is observed, that is, a species that is not included in the kinetic model.

3.1 | Identification of low-temperature species in the four investigated flames

Figure 2 shows the mass spectra obtained at 10.75 and 10 eV for the *n*-butane-doped hydrogen flame at a distance of 0.5 mm from the burner surface. This position corresponds to a flame temperature of about 708 K considering the experimental temperature profile provided by Krüger et al.[34] As mentioned above, the probe-perturbed temperature profile was obtained from the temperature dependence of the gas flow through the sampling probe by using a measured exhaust gas temperature. Peaks at *m/z* 48, 62, 76, and 90 indicate the formation of alkyl hydroperoxides under the investigated conditions in the *n*-butane/H_2 flame, while the signal at *m/z* 47 is assigned to the methylperoxy radical (CH_3OO), as discussed below. The alkyl hydroperoxides follow the trend of decreasing ionization energy with increasing number of carbon atoms. Averaging times were 240 and 600 s for the mass spectra in Figure 2 at 10.75 and 10 eV, respectively, in order to get a good signal-to-noise ratio. PIE spectra of the alkyl hydroperoxides are known from JSR measurements of various fuels, for example, dimethyl ether,[47] *n*-butane[20] or propane,[22] and are used for comparison with our flame-sampled spectra. Furthermore, the PIE spectrum of the methylperoxy radical was experimentally determined by Meloni et al.[48]

3.1.1 | Detection and identification of *m/z* 47: The methylperoxy radical (CH_3OO)

Figure 3A shows the experimental PIE spectra of *m/z* 47 in the *n*-butane/H_2 and 2-butene/H_2 flame in comparison with the measured PIE spectrum of the methylperoxy

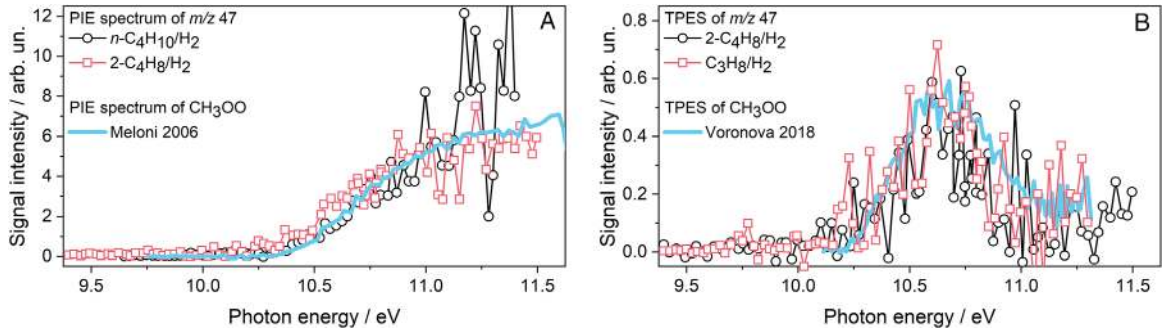

FIGURE 3 (A) Flame-sampled PIE spectra of *m/z* 47 in comparison with the PIE spectrum of the methylperoxy radical (CH_3OO) by Meloni et al.[48] (B) Flame-sampled TPE spectrum of *m/z* 47 in comparison with the TPE spectrum of the methylperoxy radical (CH_3OO) by Voronova et al.[50]

radical (CH_3OO) by Meloni et al.[48] The adiabatic ionization energy of 10.33 eV for the CH_3OO radical from Meloni et al.[48] is in good agreement with the onset of our PIE spectra confirming the formation of CH_3OO in the flame. The signal at *m/z* 47 was corrected for contributions of the ^{13}C isotope of *m/z* 46. Fragmentation of the methyl hydroperoxide to *m/z* 47 starts at higher photon energies of 11.4 eV as shown by Covert et al. who investigated the dissociative photoionization process of methyl hydroperoxide.[49] The comparison of the measured TPE spectra of *m/z* 47 from the 2-butene- and propane-doped hydrogen flame with the TPE spectrum of CH_3OO by Voronova et al.[50] also confirms clearly the formation of the CH_3OO radical in the flame as seen in Figure 3B. In low-temperature oxidation, alkylperoxy radicals are formed by oxidation of the corresponding alkyl radical with molecular oxygen. These radicals can subsequently react to alkyl hydroperoxides or isomerize (for ROO with R > CH_3) by internal hydrogen transfer to hydroperoxyalkyl radicals (QOOH), which are very weakly bound species.[13] The QOOH radical can undergo a second oxygen addition and chain branching. In the flame environment, where the temperature strongly rises, the formation of alkyl hydroperoxides is expected. No species related to the second oxygen addition, for example, keto hydroperoxides, were observed under the investigated conditions. However, the formation of alkyl hydroperoxides can be confirmed as discussed in the following. The lack of higher alkylperoxy radical signal in the measurements is not contrary to the presence of higher alkyl hydroperoxides in the flame, because these radicals have unstable cations as corroborated by Meloni et al.[48] The mass spectrometric detection is therefore not feasible.

3.1.2 | Detection and identification of *m/z* 48: Methyl hydroperoxide (CH_3OOH)

The smallest alkyl hydroperoxide is methyl hydroperoxide (CH_3OOH) with *m/z* 48. The measured PIE spectra at this mass-to-charge ratio from the *n*-butane/H_2 and 2-butene/H_2 flame are presented in Figure 4A. They show an onset slightly below 9.9 eV, which matches well to the adiabatic ionization energies of 9.77 and 9.83 eV for methyl hydroperoxide calculated at two different levels of theory by Moshammer et al.[47] They identified this hydroperoxide during oxidation of dimethyl ether in a jet-stirred reactor by photoionization mass spectrometry.[47] Their measured PIE spectrum with the onset at 9.85 eV is also shown in Figure 4A and confirms the formation of methyl hydroperoxide in the investigated flames. The only possible second isomer is methanediol ($HOCH_2OH$), which has a distinctly larger ionization energy. The calculated ionization energy of methanediol depends on its conformer and lies between 10.33 and 11 eV.[47] Because no significant rise in the PIE spectra of *m/z* 48 is observed in this energy range, the formation of detectable quantities of methanediol under our investigated conditions can be excluded at this position in the flame. Our calculation of the adiabatic ionization energy at the G4 [Ref. 51] level of theory with Gaussian 16 [Ref. 52] gives a value of 10.99 eV for the trans-conformer of methanediol. A Franck–Condon (FC) simulation at 500 K was performed with the program ezSpectrum[53] and is presented together with the TPE spectra of *m/z* 48 measured in the 2-butene/H_2 and propane/H_2 flames in Figure 4B. The TPE spectra show a rise at the adiabatic ionization energy of methyl hydroperoxide and have a broad band as observed in typical photoelectron spectra of alkanes and in the TPE spectrum of the CH_3OO radical. The FC simulation for the trans-conformer of methanediol shows a well-structured spectrum but does not overlap with our measured flame-sampled spectra. Recently, Bourgalais et al. measured a TPE spectrum of *m/z* 48 during the low-temperature oxidation of *n*-pentane in a JSR at a temperature of 585 K and identified methyl hydroperoxide.[30] Their spectrum shows a threshold at about 9.8 eV (see Figure 4B) with a slightly more pronounced maximum at 10.8 eV. The overall spectrum has a similar width as our spectrum. The presence of another conformer of methanediol could be

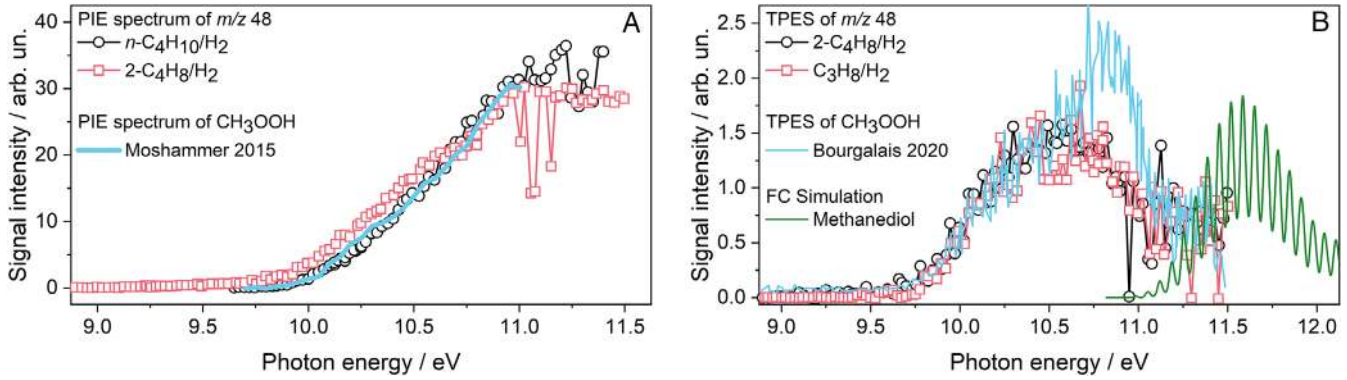

FIGURE 4 (A) Flame-sampled PIE spectra of m/z 48 in comparison with the PIE spectrum of the methyl hydroperoxide (CH_3OOH) by Moshammer et al.[47] (B) Flame-sampled TPE spectra of m/z 48 in comparison with the TPE spectrum of CH_3OOH by Bourgalais et al.[30] and a FC simulation of methanediol

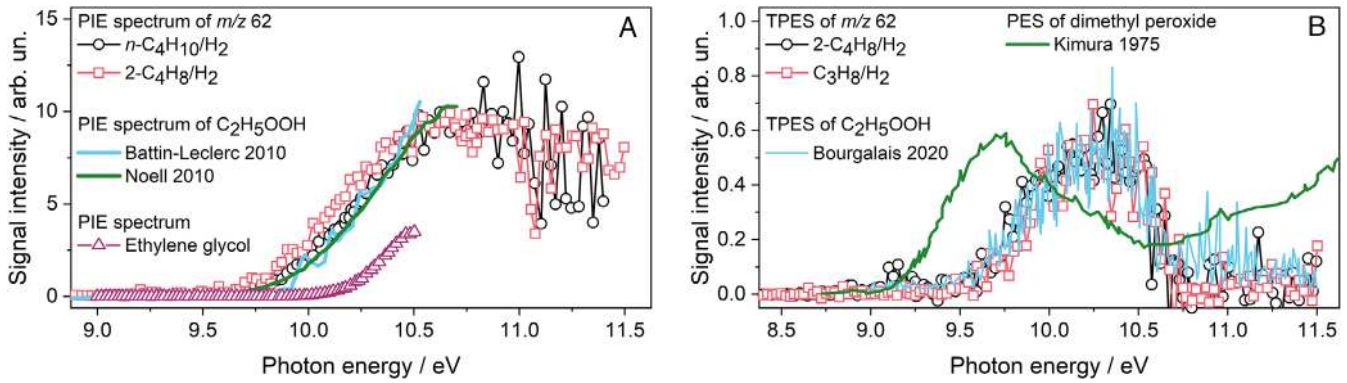

FIGURE 5 (A) Flame-sampled PIE spectra of m/z 62 in comparison with the PIE spectrum of the ethyl hydroperoxide (C_2H_5OH) by Battin-Leclerc et al.[20] and Noell[54] and our measured PIE spectrum of ethylene glycol. (B) Flame-sampled TPE spectra of m/z 62 in comparison with the TPE spectrum of C_2H_5OOH by Bourgalais et al.[30] and the PES of dimethyl peroxide by Kimura and Osafune[55]

conceivable here and may explain the differences in the spectra.

3.1.3 | Detection and identification of m/z 62: Ethyl hydroperoxide (C_2H_5OOH)

Ethyl hydroperoxide (C_2H_5OOH) with m/z 62 is the next member of the homologous series of alkyl hydroperoxides. Figure 5 shows our measured PIE spectra of m/z 62 obtained from the *n*-butane- and 2-butene-doped hydrogen flame and the TPE spectra of the same m/z ratio from the 2-butene/H_2 and propane/H_2 flame. Ethyl hydroperoxide was identified during the low-temperature oxidation of *n*-butane by Battin-Leclerc et al.[20] and their JSR-sampled PIE spectrum matches well with our flame-sampled PIE spectrum showing that ethyl hydroperoxide is also formed in flames. Noell has studied the self-reactions of C_2H_5OO by time-resolved photoionization mass spectrometry and also measured the PIE spectrum of ethyl hydroperoxide.[54] The PIE spectrum reported by Noell has the same onset at about 9.6 eV and a matching shape. The flame-sampled TPE spectra of m/z 62 from Figure 5B also match the experimental TPE spectrum of the ethyl hydroperoxide from the work of Bourgalais et al.[30] and additionally confirms the formation of this smaller alkyl hydroperoxide in the flame-sampling experiment.

Other stable, oxygenated species are theoretically possible at m/z 62, but can be excluded due to the following reasons. Isobaric species with the elemental composition CH_2O_3 have significantly higher calculated ionization energies than the observed onset, that is, 10.87 eV for methaneperoxoic acid and 11.29 eV for carbonic acid.[47] The two isomers of ethyl hydroperoxide with the elemental composition $C_2H_6O_2$ also have higher ionization energies. The PIE spectrum of ethylene glycol ($HOCH_2CH_2OH$) was directly measured by us at the Swiss Light Source and is shown in Figure 5A. The PIE spectrum does not fit to

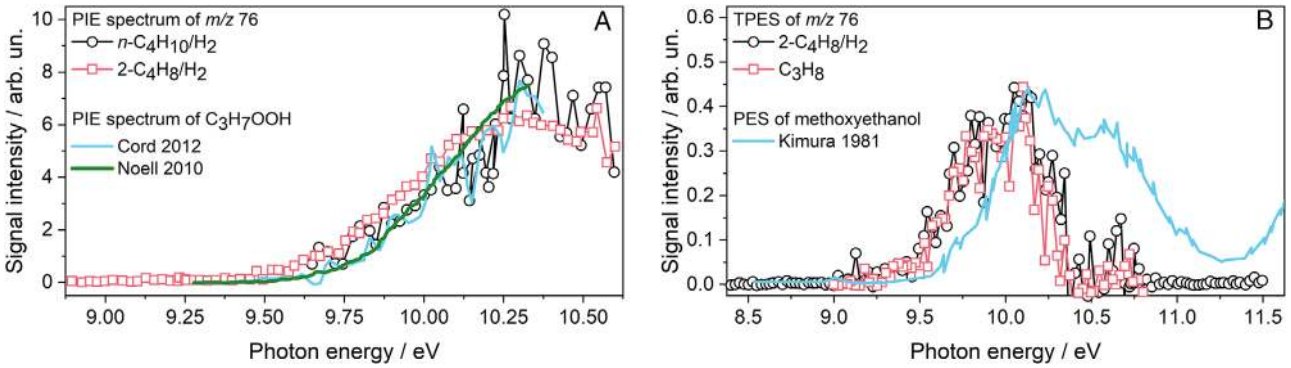

FIGURE 6 (A) Flame-sampled PIE spectra of *m/z* 76 in comparison with the PIE spectrum of propyl hydroperoxide (C_3H_7OOH) by Cord et al.[22] and Noell.[54] (B) Flame-sampled TPE spectra of *m/z* 76 in comparison with the PES of methoxyethanol by Kimura et al.[57]

the flame-sampled spectrum, and no onset at the adiabatic ionization energy is observed so that formation of ethylene glycol can be excluded. No experimental value for the ionization energy of methoxymethanol (CH_3OCH_2OH) is reported in the literature, but ionization energy of 10.05 eV calculated by Moshammer et al.[47] is higher than the observed onset. A third isomer is dimethyl peroxide (CH_3OOCH_3) with an adiabatic and vertical ionization energy of 9.1 and 9.71 eV, respectively.[55] The photoelectron spectrum (PES) of dimethyl peroxide is shown in Figure 5B, and the comparison with our measured TPE spectra clearly shows that this isomer is absent in the investigated flames. The position of the first band in the PES of dimethyl peroxide is at significantly lower photon energy than the observed band in the flame-sampled TPE spectra of *m/z* 62.

3.1.4 | Detection and identification of *m/z* 76: Propyl hydroperoxides (C_3H_7OOH)

For propyl hydroperoxide and larger alkyl hydroperoxides, regioisomers have to be considered. To clarify, the sum of *n*-propyl and isopropyl hydroperoxide is defined as propyl hydroperoxide (C_3H_7OOH). Flame-sampled PIE and TPE spectra of *m/z* 76 are presented in Figure 6. One PIE spectrum of propyl hydroperoxide was taken from the work of Cord et al., who identified intermediates at *m/z* 76 during the low-temperature oxidation of propane as the sum of both isomers and also calculated adiabatic ionization energies of 9.5 and 9.42 eV for *n*-propyl and isopropyl hydroperoxide, respectively.[22] The second PIE spectrum of propyl hydroperoxide presented in Figure 6A with the onset of 9.6 eV was measured by Noell during the dissociative ionization of the propylperoxy radical.[54] The onset in our flame-sampled PIE spectra is about 9.5 eV and in good agreement with the literature PIE spectra. One isomer with known ionization energy in the energy range of the observed onset is dimethoxymethane (methylal), but it does not have a stable parent ion at *m/z* 76 and directly undergoes dissociation losing hydrogen to form the fragment ion at *m/z* 75.[56] A second isomer is methoxyethanol ($CH_3OC_2H_5OH$) with a vertical ionization energy of 10.13 eV.[57] This value would agree with the second peak in the measured TPE spectra in Figure 6B, but the band in the PES of methoxyethanol is broader and does not match to our spectra. It is important to note that the shape of conventional photoelectron spectra can differ from the mass-selected TPE spectra, especially when the molecule undergoes dissociative photoionization. The observed sharp signal drop in the measured TPE spectra may be caused by such a dissociative photoionization process of the propyl hydroperoxides or the methoxyethanol. Therefore, the presence of methoxyethanol cannot be completely excluded. From a chemical point of view, the formation of the propyl peroxides is more likely and its formation is further supported by the matching of the literature PIE spectra and the presence of the smaller alkyl hydroperoxides, which were clearly identified. The same conclusions apply to the butyl and butenyl hydroperoxides discussed below. The two observed peaks at about 9.85 and 10.1 eV in Figure 6B may therefore represent the two propyl hydroperoxide isomers, which are formed from the reaction of the *n*-propyl and isopropyl radical with molecular oxygen. No experimental or theoretical photoelectron spectra are available in the literature for propyl hydroperoxide. Our TPE spectrum of *m/z* 43 clearly shows that both radicals, that is, *n*-propyl and isopropyl hydroperoxide, are formed in the propane-doped hydrogen flame, and the onset in the PIE spectra of *m/z* 43 from the *n*-butane- and 2-butene-doped hydrogen flame at least shows that the isopropyl radical is present (spectra not shown here).

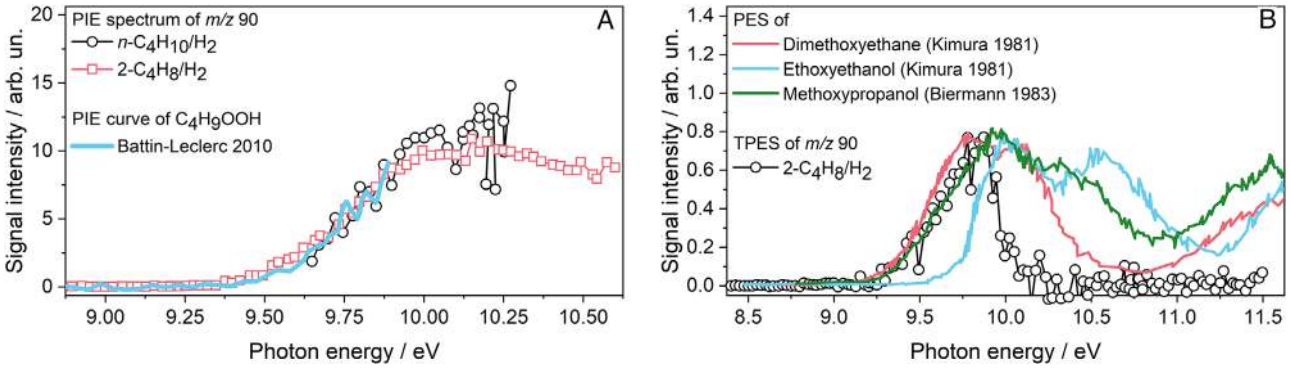

FIGURE 7 (A) Flame-sampled PIE spectra of *m/z* 90 in comparison with the PIE spectrum of butyl hydroperoxide (C_4H_9OOH) by Battin-Leclerc et al.[20] (B) Flame-sampled TPE spectra of *m/z* 90 in comparison with the photoelectron spectra of dimethoxyethane and ethoxyethanol by Kimura et al.[57] and methoxypropanol by Biermann and Morton[58]

3.1.5 | Detection and identification of *m/z* 90: Butyl hydroperoxides (C_4H_9OOH)

Butyl hydroperoxide can only be found in the C_4-doped hydrogen flames where butyl radicals are formed by hydrogen abstraction from *n*-butane or by hydrogen addition to 2-butene. Krüger et al.[34] investigated the hydrogen abstraction for the *n*-butane-doped flame in detail and observed that the secondary 2-butyl radical and the primary 1-butyl radical are formed in equal amounts with maximum mole fractions of 1.7×10^{-5}. Taking into account the number of primary and secondary C–H bonds in *n*-butane, there is a stronger preference towards abstraction of a hydrogen atom from a secondary carbon atom.[34] For the 2-butene flame, the PIE and the TPE spectra of *m/z* 57 indicate that at least the 2-butyl radical is formed (spectra not shown here). In principle, four butyl hydroperoxide isomers exist, but only the formation of 1-butyl and 2-butyl hydroperoxide is expected due to the structure of the investigated C_4 fuels. Figure 7 shows the flame-sampled PIE spectra of *m/z* 90 from the two C_4-doped hydrogen flames and the TPE spectrum of *m/z* 90 from the 2-butene/H_2 flame. Battin-Leclerc et al. investigated the oxidation of *n*-butane in a JSR and concluded that butyl hydroperoxide is formed at *m/z* 90 due to accordance with their observed onset in the PIE spectrum with calculated ionization energies of 1-butyl and 2-butyl hydroperoxide and the sharp peak in the mole fraction profile, which is typical for very reactive molecules that decompose quickly when temperature increases.[20] Their PIE spectrum matches well to our flame-sampled PIE spectra as seen in Figure 7A. Further isomers are possible, and photoelectron spectra of species with known ionization energy (IE) close to the observed onset at 9.4 eV, that is, dimethoxyethane,[57] ethoxyethanol,[57] and methoxypropanol,[58] are shown in Figure 7B in comparison to the TPE spectrum of *m/z* 90 measured in the 2-butene/H_2 flame. The first band in the photoelectron spectra of these species is significantly broader than our measured TPE spectrum, but dissociative photoionization cannot be excluded as discussed for the identification of the propyl hydroperoxides. Ashmore and Burgess recorded the photoelectron spectra of larger alkyl hydroperoxides (C_4–C_7) and measured an adiabatic ionization energy of 9.36 eV and a vertical ionization energy of 9.75 eV for 1-butyl hydroperoxide, but spectra were not reported in their work.[59] However, they mentioned that the photoelectron spectra of the *n*-alkyl hydroperoxides resemble those of the normal alcohols.[59] In addition, the values for the adiabatic and vertical ionization energy match to our measured spectra. The vertical ionization energy of *tert*-butyl hydroperoxide is 10.24 eV,[60] which is significantly higher than our measured maximum. The formation of *tert*-butyl hydroperoxide is therefore not expected, and this result corroborates our assertion that only 1-butyl and 2-butyl radicals are formed.

3.1.6 | Detection and identification of *m/z* 55 and 88: The 1-methylallyl radical and butenyl hydroperoxides

2-Butene is the only alkene whose combustion was studied here. The direct fuel radicals formed by hydrogen abstraction are C_4H_7 and the TPE spectrum in Figure 8A clearly shows that the resonance-stabilized 1-methylallyl radical is solely formed. Our measured TPE spectrum of *m/z* 55 from the 2-butene/H_2 flame perfectly matches to the experimentally determined TPE spectrum of the 1-methylallyl radical by Lang et al.[61] who used 3-penten-1-yl nitrite as precursor to generate the *z*-conformer of 1-methylallyl. They observed both conformers, because the rotational barrier for isomerization is very low.[61] Figure 8A also displays the convolution of the FC simulation for the two conformers, that is, (*E*)-1-methylallyl and (*Z*)-1-methylallyl, and their

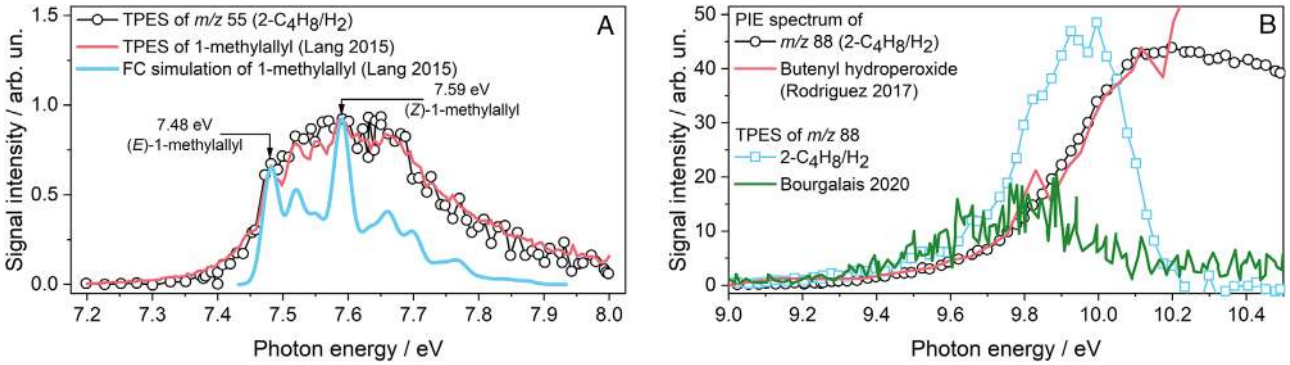

FIGURE 8 (A) Flame-sampled TPE spectrum of *m/z* 55 in comparison with a measured TPE spectrum and a FC simulation of the 1-methylallyl radical by Lang et al.[61] (B) Flame-sampled PIE and TPE spectrum of *m/z* 88 in comparison with the PIE spectrum of butenyl hydroperoxide by Rodriguez et al.[27] and a JSR-sampled TPE spectrum of *m/z* 88 from the oxidation of *n*-pentane by Bourgalais et al.[30]

adiabatic ionization energy from the work of Lang et al.[61] We used *trans*-2-butene for our flame investigations and were able to observe the formation of both conformers of the 1-methylallyl radical.

Principally, alkenyl hydroperoxides can also be formed during the low-temperature oxidation analogous to the formation of alkyl hydroperoxides. For example, Rodriguez et al. identified allyl hydroperoxide (C_3H_5OOH) at *m/z* 74, butenyl hydroperoxides (C_4H_7OOH) at *m/z* 88, and pentenyl hydroperoxides (C_5H_9OOH) at *m/z* 102 during the oxidation of *n*-pentane in a jet-stirred reactor.[27] They also detected C_3–C_7 alkenyl hydroperoxides during the oxidation of *n*-heptane and C_3–C_6 and C_9–C_{10} alkenyl hydroperoxides during the oxidation of *n*-decane.[28] From the observation that only the resonance-stabilized 1-methylallyl radical is formed in the 2-butene/H_2 flame, we would expect the formation of but-1-enyl 3-hydroperoxide and but-2-enyl 1-hydroperoxide. The PIE and TPE spectra of *m/z* 88 from the 2-butene/H_2 flame are shown in Figure 8B. The observed onset in the PIE spectrum and the general shape up to 10.2 eV fit well to the measurement of butenyl hydroperoxides in the *n*-pentane oxidation by Rodriguez et al.[27] The onset of our measured PIE spectrum is at 9.2 eV. This value is in accordance with our calculation of 9.18 eV for the adiabatic ionization energy of but-2-enyl 1-hydroperoxide. The presence of but-1-enyl 3-hydroperoxide is also possible, because the calculated ionization energy of this isomer is somewhat higher than 9.33 eV. Adiabatic ionization energies of these two isomers were calculated in this work at the CBS-QB3 level of theory with Gaussian 16.[52] Bourgalais et al. measured a TPE spectrum of *m/z* 88 during oxidation of *n*-pentane in a JSR at 585 K[30] (see Figure 8B). Since their spectrum overlapped to an FC analysis of the but-1-enyl 3-hydroperoxide, they concluded that this isomer may be formed during *n*-pentane oxidation. The onset in our TPE spectrum of *m/z* 88 matches to the onset in the JSR-sampled TPE spectrum and confirms the presence of but-1-enyl 3-hydroperoxide in the 2-butene/H_2 flame. This accordance and the well-reproduced experimental PIE spectrum by the literature data let us conclude that butenyl hydroperoxides are formed under the investigated conditions. However, the observed maximum at about 10 eV in the TPE spectrum is not reproduced and a further species may be present in the 2-butene/H_2 flame. Isomers with known ionization energies are butanoic acid, *n*-propyl formate, and methyl propionate, but their adiabatic ionization energies at 10.17, 10.54, and 10.15 eV[62] are larger than 10 eV. The mass resolution of the endstation does not allow a determination of the exact elemental composition. Besides the formation of $C_4H_8O_2$ isomers, the formation of $C_5H_{12}O$ isomers, which are mostly ethers and alcohols, is principally possible requiring further investigations. A signal at *m/z* 88 is also observed in the *n*-butane-doped hydrogen flame as seen in the mass spectrum of Figure 2B. No information about the onset in the PIE spectrum of *m/z* 88 from the *n*-butane/H_2 flame is available, because the energy scan was started above the ionization energy of the butenyl hydroperoxides. Due to the observation of the 1-methylallyl radical in the *n*-butane/H_2 flame, the formation of butenyl hydroperoxides can be inferred as likely in this flame.

3.1.7 | Detection and identification of *m/z* 44 and 58: Cyclic ethers and common oxygenates

Besides the formation of alkyl hydroperoxides from alkylperoxy radicals, chain-propagation of QOOH radicals is also likely in the low-temperature oxidation and may lead to cyclic ethers and OH,[13] for example, oxetane and methyloxirane from $CH_2CH_2CH_2OOH$ and

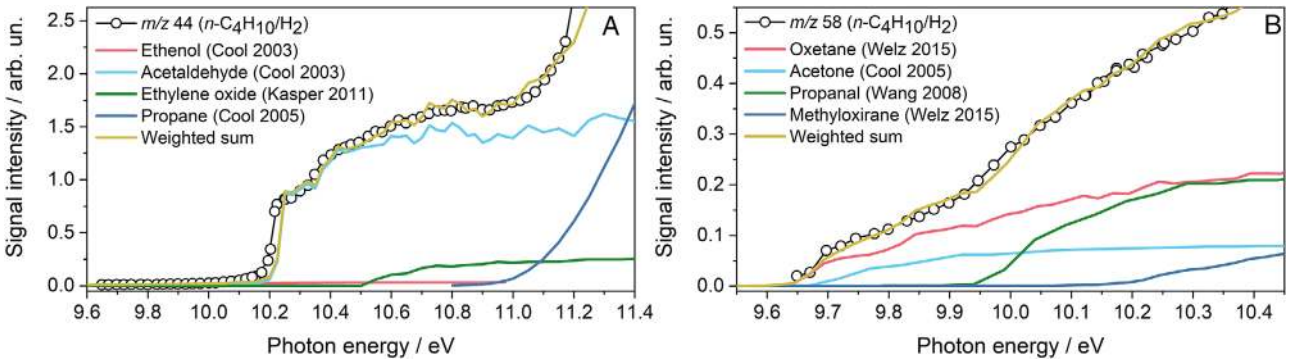

FIGURE 9 (A) PIE spectrum of *m/z* 44 from the *n*-butane/H_2 flame in comparison with PIE spectra of ethenol,[63] acetaldehyde,[63] ethylene oxide,[64] and propane[65] and with a weighted sum. (B) PIE spectrum of *m/z* 58 from the *n*-butane/H_2 flame in comparison with PIE spectra of oxetane,[23] acetone,[66] propanal,[67] and methyloxirane,[23] and with a weighted sum

CH_3CHCH_2OOH, respectively. The QOOH radicals are generally formed by isomerization via internal hydrogen abstraction from the corresponding alkylperoxy radical.[13] Therefore, the observation of cyclic ethers would be further evidence for the low-temperature oxidation in flames. Figure 9 displays the flame-sampled PIE spectra of *m/z* 44 and 58. Oxygenated three- and four-ring species are expected at these mass-to-charge ratios during low-temperature oxidation. For *m/z* 44, the best fit is a weighted sum of the photoionization spectra of ethenol,[63] acetaldehyde,[63] ethylene oxide,[64] and propane.[65] Considering only the three C_2H_4O isomers, the percentages are 1.4% ethenol, 83% acetaldehyde, and 15.6% ethylene oxide. Only one cyclic ether can be formed from the OH loss of C_2H_4OOH, while for C_3H_6OOH two regioisomers are possible and the formation of oxetane and methyloxirane must be considered. The flame-sampled PIE spectrum is the best fit of the PIE spectra of oxetane,[23] acetone,[66] propanal,[67] and methyloxirane[23] in the energy range of 9.65 and 10.35 eV. The percentages for the four isomers at this position (i.e., HAB of 0.5 mm) in the energy scan are 38.4% for oxetane, 10.8% for acetone, 35.4% for propanal, and 15.4% for methyloxirane. Mole fraction profiles of oxetane and methyloxirane could not be separated from acetone and propanal, respectively. However, reliable mole fraction profiles of the two isomer pairs oxetane and acetone and methyloxirane and propanal are determined with the ratios from the energy scan. At 0.5 mm, the mole fractions are 1.4×10^{-4} (oxetane and acetone) and 5.4×10^{-5} (methyloxirane and propanal). These values show the relevance of low-temperature oxidation products under the investigated conditions. PIE spectra of both *m/z* 44 and 58 reveal contributions of cyclic ethers, that is, ethylene oxide, oxetane, and methyloxirane. Rate of production analyses at HAB of 0.5 and 0.75 mm indicate that ethylene oxide is directly formed from the ethylperoxy radical ($C_2H_5O_2 = C_2H_4O1\text{-}2 + OH$), while oxetane and methyloxirane originate from the decomposition of C_3H_6OOH radicals. In detail, oxetane ($C_3H_6O1\text{-}3$) is only formed by decomposition of the $CH_2CH_2CH_2OOH$ radical ($C_3H_6OOH1\text{-}3 = C_3H_6O1\text{-}3 + OH$) and methyloxirane ($C_3H_6O1\text{-}2$) from decomposition of CH_3CHCH_2OOH ($C_3H_6OOH1\text{-}2 = C_3H_6O1\text{-}2 + OH$) and $CH_2CH(CH_3)OOH$ radicals ($C_3H_6OOH2\text{-}1 = C_3H_6O1\text{-}2 + OH$). Welz et al. also concluded for the low-temperature oxidation of propane that the oxygenated cyclic species oxetane and methyloxirane can only be formed by QOOH radicals.[23] Thus, the observation of these species is an indication of the low-temperature chemistry in our investigated flame.

3.1.8 | Detection and identification of *m/z* 72 and 86: Ketones

Besides the formation of expected small oxygenated combustion intermediates like formaldehyde and acetaldehyde, larger C_4 oxygenates were identified by their photoelectron spectra in the 2-butene/H_2 flame as shown in Figure 10. The recorded TPE spectrum of *m/z* 72 has an intensive peak at 9.52 eV and a smaller band at 9.67 eV. The TPE spectrum of butanone ($C_2H_5COCH_3$) measured by Kercher et al.[68] fits perfectly to the flame-sampled spectrum indicating that this species is formed in the flame at HAB of 0.5 mm. The formation of butanone may result from the decomposition of the 2-C_4H_8OOH radical and competes with the formation of cyclic ethers (2,3-dimethyloxirane, 2-methyloxetane, or 2-ethyloxirane).[26] The ionization energy of 2-methyloxetane is close to the value of butanone, while 2,3-dimethyloxirane (9.8 eV) and 2-ethyloxirane have higher ionization energies.[26] Our spectrum does not show any contributions from other species at *m/z* 72. Similar observations were made for the

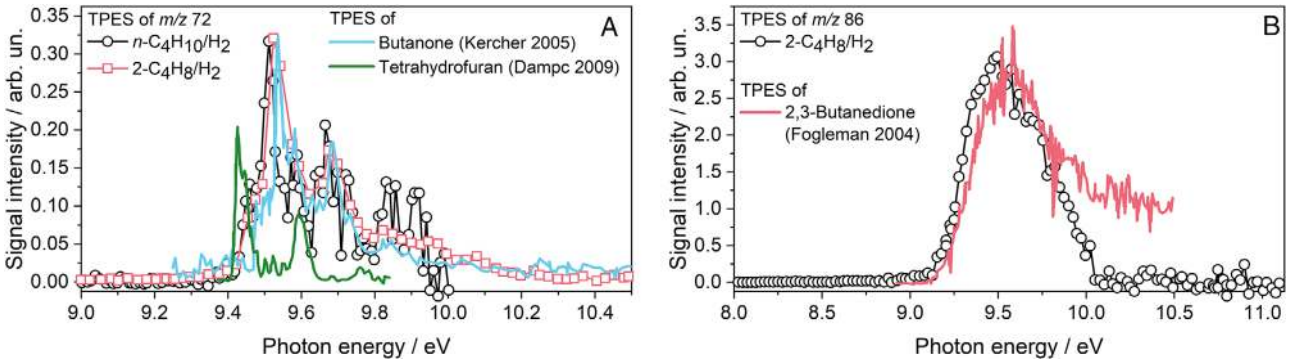

FIGURE 10 TPE spectra of *m/z* 72 and 86 recorded in C_4 hydrocarbon-doped flames in comparison with the TPE spectra of tetrahydrofuran,[69] butanone,[68] and 2,3-butanedione[70]

n-butane/H_2 flame. The TPE spectrum of *m/z* 72 from the *n*-butane-doped hydrogen flame is also plotted in Figure 10. However, peak positions of the two major bands of butanone could not be replicated sufficiently. There is a redshift of about 0.02 eV, but the peak intensities are well represented. This spectrum was recorded at HAB of 0.75 mm. As already discussed, 1-butyl and 2-butyl radicals are formed in the oxidation of *n*-butane. Additional decomposition products of the 1-C_4H_8OOH must therefore be considered, for example, tetrahydrofuran (THF) and *n*-butanal (C_3H_7CHO). Ionization energies of THF and *n*-butanal are 9.4 and 9.82 eV, respectively.[62] The TPE spectrum of THF measured by Dampc et al.[69] mismatches our flame-sampled TPE spectrum (see Figure 10). No information about the PE or TPE spectrum of 2-methyloxetane is given in the literature. Since its ionization energy is close to butanone, minor contributions cannot be excluded. Eskola et al. investigated detailed product formation in the low-temperature oxidation of *n*-butane by using deuterated butane (*n*-butane-d_6 and *n*-butane-d_4) in time-resolved experiments.[26] When considering their individual photoionization spectra of C_4H_8 isomers, our PIE spectrum of *m/z* 72 from the *n*-butane/H_2 flame is best represented by a weighted sum of butanone and 2-methyloxirane up to the ionization energy of *n*-butanal (spectrum not shown here). However, butanone seems to be the major combustion intermediate at *m/z* 72 for both C_4 fuels. Butanone was also the sole combustion product at *m/z* 72 in the low-temperature oxidation of *n*-pentane.[30]

2,3-Butanedione ($C_4H_6O_2$), also known as diacetyl, is a second C_4 oxygenate, which can be identified by its TPE spectrum (see Figure 10). The spectrum was recorded in the 2-butene/H_2 flame and is well represented by the TPE spectrum of the pure substance by Fogleman et al.[70] A small difference can be seen starting from 9.85 eV, where our spectrum drops more sharply. The spectrum differs from butanone and has a very broad band. The ionization energy was determined to be 9.21 eV.[70] The TPE spectrum of *m/z* 86 in the *n*-butane/H_2 flame had a low signal-to-noise ratio, but the shape of the PIE curve and the onset at about 9.2 eV agree with the PIE spectrum from the 2-butene/H_2 flame. It is therefore likely that 2,3-butanedione is also the major combustion intermediate at *m/z* 86 in the *n*-butane/H_2 flame under the investigated conditions.

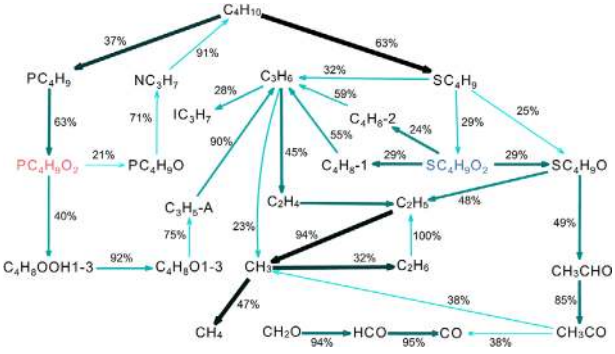

FIGURE 11 Reaction path analysis for the *n*-butane/H_2 flame at HAB of 1 mm (766 K). Thickness of arrows represents the carbon flux from one species to another. Only carbon fluxes above 10% of the total carbon flux are shown. Percentages next to arrows give individual contributions to the consumption of a species

3.2 | Reaction path analysis and quantification of low-temperature species in the *n*-butane-doped hydrogen flame

Figure 11 shows a reaction path analysis for the *n*-butane/H_2 flame to identify the main consumption pathway of the fuel. The analysis was done for a HAB of 1 mm at 766 K, where the temperature is still in the low-temperature regime and half of the *n*-butane is already consumed. The thickness of the arrows represents the carbon flux from one species to another. Only carbon fluxes above 10% of the total flux are presented. Percentages

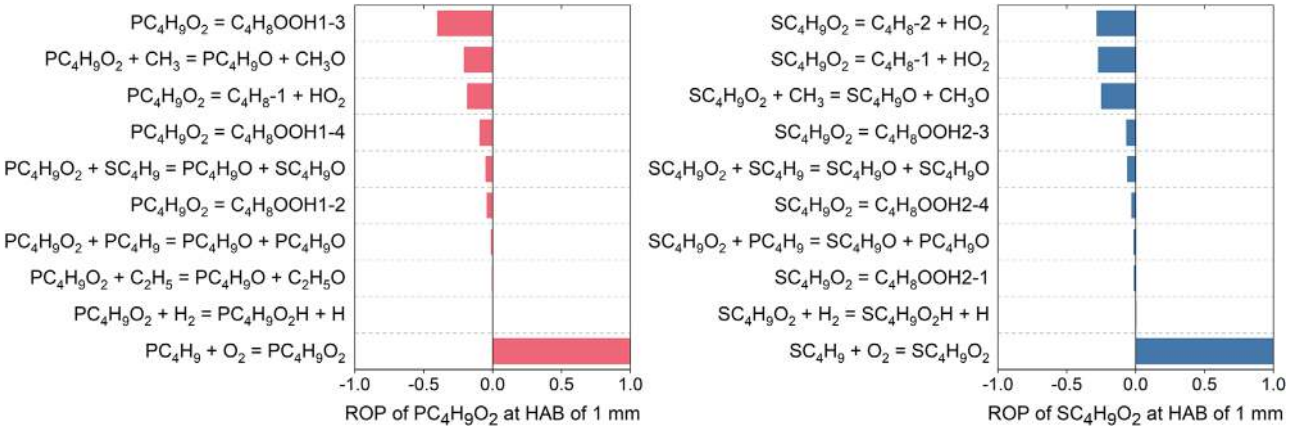

FIGURE 12 Rate of production analyses of the 1-butylperoxy ($PC_4H_9O_2$) and 2-butylperoxy radical ($SC_4H_9O_2$)

next to arrows give individual contributions to the consumption of a species. Fuel decay starts by hydrogen abstraction, preferably forming 2-butyl radicals (SC_4H_9). The ratio between 1-butyl (PC_4H_9) and 2-butyl radicals is about 40:60. For both fuel radicals, the formation of the corresponding butylperoxy radical by reaction with molecular oxygen is the main consumption pathway, that is, the 1-butylperoxy ($PC_4H_9O_2$) and 2-butylperoxy radical ($SC_4H_9O_2$) from the 1-butyl and 2-butyl radical, respectively.

Smaller alkylperoxy radicals and C_1–C_4 alkyl hydroperoxides seem to play a minor role in the mechanism in terms of the total carbon flow. From the general low-temperature oxidation mechanism as shown in Figure 1, it is expected that the butylperoxy radicals react with HO_2 to butyl hydroperoxides and O_2, decompose to butenes and HO_2 or isomerize to hydroperoxybutyl radicals. In the AramcoMech 2.0, only the latter two pathways are relevant as demonstrated by rate of production analyses of the two butylperoxy radicals (see Figure 12). Both C_4H_9OO radicals are exclusively formed by the reaction of molecular oxygen with the 1-butyl and 2-butyl radical, respectively. Isomerization to hydroperoxybutyl radicals (C_4H_8OOH1-3 and C_4H_8OOH1-4), decomposition to 1-butene (C_4H_8-1) and HO_2, and reaction with CH_3 to the 1-butoxy (PC_4H_9O) and methoxy radical (CH_3O) are the major sinks for the 1-butylperoxy radical. The decomposition of the 2-butylperoxy radical also largely leads to the formation of 1-butene and HO_2 as shown by Figure 12. In addition, 2-butene and HO_2 are formed by unimolecular decomposition and the 2-butoxy and methoxy radical by reaction with the methyl radical. A stronger impact of the low-temperature oxidation in the investigated flame than predicted by the model may be an explanation for the deviations of the mole fractions of propene, 1-butene, and 2-butene. When O_2 addition to the 2-butyl radical is more favored than hydrogen abstraction, the concentration of both butene isomers would be higher and that of propene lower as observed. Since the alkyl hydroperoxides were observed (see Section 3.1), they may also be an indicator of the importance of the low-temperature oxidation.

The butyl hydroperoxides are mainly formed by the reaction of the 1-butylperoxyl or 2-butylperoxyl radical with HO_2 as shown in the general low-temperature oxidation scheme. But compared to the other branching agents, they play only a minor role in the mechanism. Mole fractions of the butylperoxy radicals are more than two orders of magnitude higher than for the butyl hydroperoxides. Since the direct measurement of larger alkylperoxy radicals by mass spectrometry is due to their unstable cations not possible, it is beneficial that the alkyl hydroperoxides seem to be formed only by one reaction from the alkylperoxy radicals. The position and magnitude of the alkyl hydroperoxides are directly related to the alkylperoxy radical profiles so that it can be used to indirectly validate the simulated profiles of the alkylperoxy radicals. For the further breakdown of the two butoxy radicals, only two reactions are important. The 1-butoxy radical decomposes to the *n*-propyl radical (NC_3H_7) and formaldehyde (CH_2O), while the ethyl radical (C_2H_5) and acetaldehyde (CH_3CHO) are formed from the 2-butoxy radical. This means that two smaller alkyl radicals are formed, which may subsequently undergo low-temperature oxidation. But in contrast to the stable species in Figure S2, the photoionization cross sections of the alkyl hydroperoxides are unknown and must be estimated. Ashmore and Burgess have shown that the photoelectron spectra of the C_4–C_7 1-hydroperoxides resemble those of the normal alcohols.[59] Based on this observation, we quantified the mole fractions of the alkyl hydroperoxides in the *n*-butane-doped hydrogen flame by using photoionization cross sections of the structurally similar alcohols, that is, photoionization cross sections of methanol,

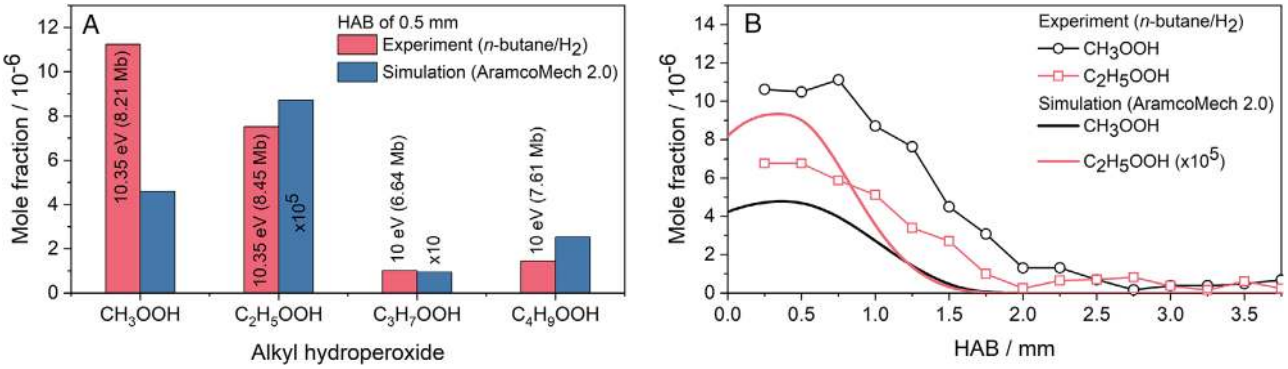

FIGURE 13 (A) Quantification of alkyl hydroperoxides in the *n*-butane-doped hydrogen flame from the energy scan measured at HAB of 0.5 mm and (B) mole fraction profiles of methyl and ethyl hydroperoxide in comparison with the results of the AramcoMech 2.0

ethanol, and 1-propanol by Cool et al.[66] and 1-butanol from the work of Xie et al.[71] Methyl and ethyl hydroperoxide are quantified at 10.35 eV, while a photon energy of 10 eV is used for propyl and butyl hydroperoxide. The photon energies are 0.5–0.7 eV above the ionization energies of the alkyl hydroperoxides, where fragmentation may be negligible. Distinct dissociative photoionization starts at higher photon energies as seen from the measured photoelectron spectra of the alkyl hydroperoxides. The total photoionization cross sections of the corresponding alcohol without considering fragmentation is therefore used for quantification. Figure 13 displays the calculated mole fractions of the C_1–C_4 alkyl hydroperoxides from the energy scan measured at HAB of 0.5 mm in the *n*-butane/H_2 flame and the mole fraction profiles of methyl and ethyl hydroperoxide from this flame. Measured mole fractions of alkyl hydroperoxides are about 10^{-5}–10^{-6} and are compared to the simulation results of the AramcoMech 2.0 in Figure 13. C_3H_7OOH represents the sum of *n*-propyl and isopropyl hydroperoxide and C_4H_9OOH the sum of 1-butyl and 2-butyl hydroperoxide, neglecting *tert*-butyl and isobutyl hydroperoxide, which play no role in the combustion of *n*-butane.

The modeling results also confirm that some hydroperoxides are formed in detectable concentrations close to the burner, where the flame temperature is lower. Mole fractions of methyl and butyl hydroperoxide have the same order of magnitude in experiment and simulation, while the mole fractions of propyl hydroperoxide and ethyl hydroperoxide are clearly underestimated. It is interesting to note that ethyl hydroperoxide is actually not formed at all according to the mechanism under our investigated conditions, whereas in the experiment the mole fraction is almost as high as that of the methyl hydroperoxide. The reaction path analysis in Figure 11 shows that the reaction of $C_2H_5 + H = CH_3 + CH_3$ is the major sink of ethyl radicals. This also applies to positions closer to the burner. Therefore, the consumption pathway of ethyl radicals by O_2 addition to form the ethylperoxy radical is not as relevant as for the butyl radicals. This behavior can explain the observed differences in the mole fraction of ethyl hydroperoxide. Zhang et al. demonstrated that O_2 addition is an important consumption pathway of the ethyl radical in an ethylene flame close to the burner at temperatures of 755 K and that the subsequent reaction of the C_2H_5OO radical is a source of ethyl hydroperoxide.[33] Overall, experimental mole fractions of alkyl hydroperoxides are typically higher than the modeling results except for butyl hydroperoxides. Caution has to be exerted in the interpretation of the mole fraction because photoionization cross sections of the alkyl hydroperoxides are unknown, and the mole fractions have higher uncertainties. Theoretical calculation of the photoionization cross section of methyl hydroperoxide by Moshammer et al.[72] shows that the cross section might be even lower than our assumed value based on methanol. The experimental mole fraction would be even bigger with a smaller photoionization cross section causing a bigger discrepancy between experimental and simulated results.

Besides the ethyl and propyl hydroperoxide, mole fractions of further oxygenated species, whose formation may be affected by the low-temperature oxidation pathways, are underestimated by the model. Their mole fraction profiles are presented in Figure 14. For example, the maximum mole fraction of ethanol is 2.7×10^{-4} at HAB of 0.5 mm in our investigated *n*-butane/H_2 flame compared to 1×10^{-6} in the simulation. The two most important reactions for the formation of ethanol (C_2H_5OH) at 0, 0.5, and 1 mm are $C_2H_5 + OH = C_2H_5OH$ and $CH_3 + CH_2OH = C_2H_5OH$ in the reaction mechanism. Low-temperature oxidation was observed by Zhang et al. in an ethylene flame.[33] They observed that the formation of ethanol was influenced by the low-temperature chemistry and identified the reaction $C_2H_5OO + OH = C_2H_5OH + O_2$ as the main source of ethanol at low temperatures.[33] However, the simulated

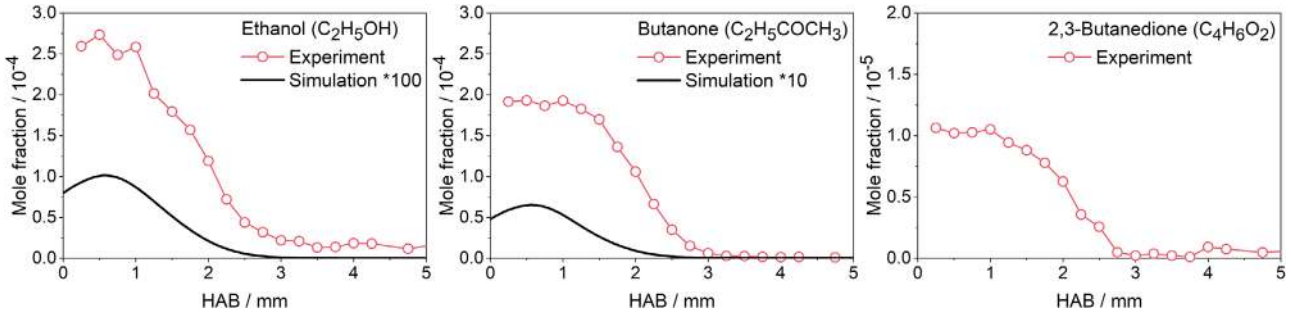

FIGURE 14 Experimental mole fraction profiles of ethanol (C_2H_5OH), butanone ($C_2H_5COCH_3$), and 2,3-butanedione ($C_4H_6O_2$) in the *n*-butane/H_2 flame compared to modeling results

mole fraction of the ethylperoxy radical is orders of magnitude smaller than for the other alkylperoxy radicals under the investigated conditions. The absence of this radical may be a reason for the underestimated mole fraction of ethanol. Since we clearly observed the ethyl hydroperoxide, the presence of the ethylperoxy radical is also likely and can explain the higher experimental mole fraction of ethanol.

The two QOOH radicals C_4H_8OOH1-3 and C_4H_8OOH1-4 decompose in the further reaction progress into 2-methyloxetane (C_4H_8O1-3) and THF, respectively. In our C_4 flames, butanone is the main C_4H_8O isomer. The maximum experimental mole fraction of butanone is 1.9×10^{-4} in the *n*-butane-doped hydrogen flame. In contrast, the simulated maximum mole fraction of butanone is only 6.5×10^{-6}, which is about 30 times lower compared to the experimental value. Since its photoionization cross section is unknown, we used the photoionization cross section of the chemically similar species *n*-butanal by Yang et al.[56] to calculate the mole fraction. The main formation pathway of butanone in the mechanism is the unimolecular decomposition of the 2-butoxy radical (SC_4H_9O), but its total contribution to the carbon flow is small. Further major consumption pathways of butanone are hydrogen abstractions followed by β-C-C-scission to yield $C_2H_4 + CH_3CO$ and $C_2H_4 + CH_2CO$ (ketene). The second C_4 oxygenate is 2,3-butanedione with an experimental mole fraction of 1.15×10^{-5} calculated using the photoionization cross section of *n*-butanal. The maximum mole fraction of 2,3-butanedione is about one order of magnitude lower than for butanone. 2,3-Butanedione and butanone may be formed from oxidation of 2-butanol as shown by Togbé et al.[73] in jet-stirred reactor measurements. 2-Butanol is formed in both investigated C_4 flames. In high-temperature combustion, consumption of 2,3-butanedione leads to ketene as shown by Sun et al. for a laminar premixed, low-pressure flame of 2,3-butanedione investigated by photoionization mass spectrometry.[74] Ketene (CH_2CO) is also formed from acetaldehyde (CH_3CHO) by the reaction sequence $CH_3CHO \rightarrow CH_3CO \rightarrow CH_2CO$. Since the mole fraction of acetaldehyde is significantly higher than that of 2,3-butanedione, the contribution to ketene formation may play a minor role compared to acetaldehyde.

Our measurements suggest that smaller hydroperoxides seem to play a more important role than the larger ones and LTC may have an influence on the formation of some oxygenated species in flames. The formation of C_1–C_4 alkyl hydroperoxides was also observed by Zhang et al.[33] in ethylene, ethane, propene, and *n*-butane flames by photoionization molecular-beam mass spectrometry. Here, we additionally measured the butenyl hydroperoxides and cyclic ethers, which also originate from low-temperature chemistry, in hydrocarbon-doped hydrogen flames. Alkyl hydroperoxides are not only identified by PIE spectra, but also by their TPE spectra. The methylperoxy radical (CH_3OO) is measured for the first time in laminar premixed flames. Measurements at different burner positions indicate that the alkyl hydroperoxides are only formed very close to the burner, where the perturbation of the probe is especially strong, and rapidly decomposes when the temperature increases. In general, the sampling probe lowers the temperature of the flame as experimentally determined in several works[75–78] and recently by Zhang et al.[33] during the investigation of the contribution of the low-temperature chemistry in a premixed, low-pressure ethylene flame. However, there are further aspects that may influence the particular temperature history of the sampled gas. Zhang et al. concluded that future investigations of geometry effects of sampling probe influence on the flame chemistry are warranted.[33] Such effects may be spatial in nature, and investigation should include effects of dimensionality assumptions on flame perturbation. This view is corroborated by two-dimensional (2D) fluid dynamics simulations, which provide deep insights into the sampling procedure,[79,80] and by the findings of Hansen et al.,[81] who investigated the probe perturbations on the temperature field one- and two-dimensionally by means of X-ray fluorescence. Recent 2D simulations of the sampling situation in a molecular-beam setup by Karakaya et al.[82] indicate that the suction effect of the probe is a decisive

disturbance of the flame structure, that is, gases are also sampled up- and downstream of the probe orifice and on the centerline in front of the probe, suction pulls a gas sample towards the probe orifice which leads to deformed temperature isolines. This suction effect overlaps with the general cooling effect of the sampling probe, but is not sufficiently considered in nozzle-perturbed temperature profiles used in one-dimensional simulations and can especially explain deviations close to the burner.[82] The limits of one-dimensional simulations for peroxide species are beyond the scope of this study but must be investigated in future work.

4 | CONCLUSIONS

PEPICO spectroscopy in combination with photoionization molecular-beam mass spectrometry is a powerful analytical tool to achieve high sensitivity to elusive species. Thanks to this technique, alkyl hydroperoxides and the methylperoxy radical are clearly identified by their PIE curves and photoelectron spectra in laminar premixed alkane- and alkene-doped hydrogen flames and even in a neat propane flame. The observation and identification of these low-temperature species in a flame environment are a hint for the low-temperature oxidation under these conditions. To the best of our knowledge, the measurement of TPE spectra of the larger alkyl hydroperoxides, that is, propyl- and butyl-hydroperoxides, has not yet been reported in the literature. Cyclic ethers are decomposition products of hydroperoxyalkyl radicals (QOOH) and are identified in the *n*-butane-doped hydrogen flame. They also serve as markers that the low-temperature oxidation may play a role at flame conditions.

The formation of higher C_4 oxygenates and ethanol might be influenced by the low-temperature oxidation and is observed in significantly larger extent than in the simulation results of the AramcoMech 2.0. Low-temperature oxidation chemistry is often neglected in flame simulations. The present results indicate at least the presence of reaction channels of this type and should be included when modeling laminar premixed low-pressure flames to consider all relevant formation pathways of those oxygenated species. For example, the detected diketone, 2,3-butanedione, is not at all considered in the mechanism and its formation can be explained by low-temperature chemistry via 2-butanol. For the *n*-butane/H_2 flame, a comprehensive dataset of mole fraction profiles for low-temperature and high-temperature oxidation products is provided. This dataset may serve for future model validation. It can help to improve the chemical modeling of the kinetics of transition from low-temperature to high-temperature oxidation in flames in a complex combustion environment that includes up- and downstream diffusion of the reactive species.

It should be noted that the peroxide species are only formed close to the burner, where the flame temperature is low and the flame perturbation by the sampling probe plays a significant role. Nevertheless, it cannot be concluded that the formation of the observed alkyl hydroperoxides is the result of the introduction of the sampling probe only. The detection of these species in a flame is a great opportunity to investigate the impact of the transition of the low-temperature oxidation to intermediate and high-temperature oxidation. It can also be stated that for a reliable model simulation, the probe-disturbance needs to be considered. As initial approach, the disturbed temperature profile is included in the provided dataset. Quantitative information is given for the alkyl hydroperoxides in the *n*-butane-doped hydrogen flame with mole fractions on the order of 10^{-5}-10^{-6}. Simulations with the perturbed temperature profile show that alkyl hydroperoxides are formed very close to the burner and some of them in detectable amounts. In future work, quantification of hydroperoxides in the other flames will give further insights into the low-temperature oxidation chemistry in flame-sampling experiments.

ACKNOWLEDGMENTS

The authors gratefully acknowledge Luka Debenjak for technical assistance and Andras Bodi for experimental research support. All authors thank the German Research Foundation (DFG) for financial support under contract KA3871/3-2 and KO4786/2-2. Patrick Hemberger thanks the Swiss Federal Office of Energy for financial support under contract SI/501269-01. The research leading to these results has received funding from the European Community's Seventh Framework Program (FP7/2007-2013) under grant agreement no. 312284. The experiments were performed at the Swiss Light Source of the Paul Scherrer Institute in Villigen, Switzerland.

DATA AVAILABILITY STATEMENT

The data that supports the findings of this study are available in the Supporting Information of this article.

REFERENCES

1. Bergthorson JM, Thomson MJ. A review of the combustion and emissions properties of advanced transportation biofuels and their impact on existing and future engines. *Renewable Sustainable Energy Rev*. 2015;42:1393-1417.
2. Geng P, Cao E, Tan Q, Wei L. Effects of alternative fuels on the combustion characteristics and emission products from diesel engines: a review. *Renewable Sustainable Energy Rev*. 2017;71:523-534.
3. Taamallah S, Vogiatzaki K, Alzahrani FM, Mokheimer EMA, Habib MA, Ghoniem AF. Fuel flexibility, stability and

emissions in premixed hydrogen-rich gas turbine combustion: technology, fundamentals, and numerical simulations. *Appl Energy*. 2015;154:1020-1047.
4. Nemitallah MA, Rashwan SS, Mansir IB, Abdelhafez AA, Habib MA. Review of novel combustion techniques for clean power production in gas turbines. *Energy Fuels*. 2018;32:979-1004.
5. Jacobs TJ, Assanis DN. The attainment of premixed compression ignition low-temperature combustion in a compression ignition direct injection engine. *Proc Combust Inst*. 2007;31:2913-2920.
6. Agarwal AK, Singh AP, Maurya RK. Evolution, challenges and path forward for low temperature combustion engines. *Prog Energy Combust Sci*. 2017;61:1-56.
7. Pachiannan T, Zhong W, Rajkumar S, He Z, Leng X, Wang Q. A literature review of fuel effects on performance and emission characteristics of low-temperature combustion strategies. *Appl Energy*. 2019;251:113380.
8. Krishnamoorthi M, Malayalamurthi R, He Z, Kandasamy S. A review on low temperature combustion engines: performance, combustion and emission characteristics. *Renewable Sustainable Energy Rev*. 2019;116:109404.
9. Ju Y, Reuter CB, Yehia OR, Farouk TI, Won SH. Dynamics of cool flames. *Prog Energy Combust Sci*. 2019;75:100787.
10. Kohse-Höinghaus K. Combustion chemistry diagnostics for cleaner processes. *Chem – Eur J*. 2016;22:13390-13401.
11. Curran HJ. Developing detailed chemical kinetic mechanisms for fuel combustion. *Proc Combust Inst*. 2019;37:57-81.
12. Wang Z, Herbinet O, Hansen N, Battin-Leclerc F. Exploring hydroperoxides in combustion: history, recent advances and perspectives. *Prog Energy Combust Sci*. 2019;73:132-181.
13. Zádor J, Taatjes CA, Fernandes RX. Kinetics of elementary reactions in low-temperature autoignition chemistry. *Prog Energy Combust Sci*. 2011;37:371-421.
14. Wang Z, Zhang L, Moshammer K, et al. Additional chain-branching pathways in the low-temperature oxidation of branched alkanes. *Combust Flame*. 2016;164:386-396.
15. Wang Z, Chen B, Moshammer K, et al. *n*-Heptane cool flame chemistry: unraveling intermediate species measured in a stirred reactor and motored engine. *Combust Flame*. 2018;187:199-216.
16. Battin-Leclerc F, Bourgalais J, Gouid Z, et al. Chemistry deriving from OOQOOH radicals in alkane low-temperature oxidation: a first combined theoretical and electron-ion coincidence mass spectrometry study. *Proc Combust Inst*. 2021;38:309-319.
17. DeCorpo JJ, McDowell MV, Sheinson RS, Wyatt JR. Quantitative measurement of methyl hydroperoxide in the acetaldehyde cool flame. *J Chem Soc, Chem Commun*. 1974:533-534.
18. Taylor GW. Peroxides in the combustion of isobutane. *Can J Chem*. 1958;36:1213-1216.
19. Herbinet O, Battin-Leclerc F. Progress in understanding low-temperature organic compound oxidation using a jet-stirred reactor. *Int J Chem Kinet*. 2014;46:619-639.
20. Battin-Leclerc F, Herbinet O, Glaude PA, et al. Experimental confirmation of the low-temperature oxidation scheme of alkanes. *Angew Chem, Int Ed*. 2010;49:3169-3172.
21. Herbinet O, Battin-Leclerc F, Bax S, et al. Detailed product analysis during the low temperature oxidation of n-butane. *Phys Chem Chem Phys*. 2011;13:296-308.
22. Cord M, Husson B, Lizardo Huerta JC, et al. Study of the low temperature oxidation of propane. *J Phys Chem A*. 2012;116:12214-12228.
23. Welz O, Burke MP, Antonov IO, et al. New insights into low-temperature oxidation of propane from synchrotron photoionization mass spectrometry and multiscale informatics modeling. *J Phys Chem A*. 2015;119:7116-7129.
24. Cord M, Sirjean B, Fournet R, Tomlin A, Ruiz-Lopez M, Battin-Leclerc F. Improvement of the modeling of the low-temperature oxidation of *n*-butane: study of the primary reactions. *J Phys Chem A*. 2012;116:6142-6158.
25. Bahrini C, Morajkar P, Schoemaecker C, et al. Experimental and modeling study of the oxidation of *n*-butane in a jet stirred reactor using cw-CRDS measurements. *Phys Chem Chem Phys*. 2013;15:19686-19698.
26. Eskola AJ, Welz O, Savee JD, Osborn DL, Taatjes CA. Synchrotron photoionization mass spectrometry measurements of product formation in low-temperature *n*-butane oxidation: toward a fundamental understanding of autoignition chemistry and n-$C_4H_9 + O_2$/s-$C_4H_9 + O_2$ reactions. *J Phys Chem A*. 2013;117:12216-12235.
27. Rodriguez A, Herbinet O, Wang Z, et al. Measuring hydroperoxide chain-branching agents during *n*-pentane low-temperature oxidation. *Proc Combust Inst*. 2017;36:333-342.
28. Rodriguez A, Herbinet O, Meng X, et al. Hydroperoxide measurements during low-temperature gas-phase oxidation of *n*-heptane and *n*-decane. *J Phys Chem A*. 2017;121:1861-1876.
29. Meng X, Rodriguez A, Herbinet O, Wang T, Battin-Leclerc F. Revisiting 1-hexene low-temperature oxidation. *Combust Flame*. 2017;181:283-299.
30. Bourgalais J, Gouid Z, Herbinet O, et al. Isomer-sensitive characterization of low temperature oxidation reaction products by coupling a jet-stirred reactor to an electron/ion coincidence spectrometer: case of *n*-pentane. *Phys Chem Chem Phys*. 2020;22:1222-1241.
31. Westbrook CK. Chemical kinetics of hydrocarbon ignition in practical combustion systems. *Proc Combust Inst*. 2000;28:1563-1577.
32. Bahrini C, Herbinet O, Glaude P-A, Schoemaecker C, Fittschen C, Battin-Leclerc F. Quantification of hydrogen peroxide during the low-temperature oxidation of alkanes. *J Am Chem Soc*. 2012;134:11944-11947.
33. Zhang X, Zhang Y, Li T, et al. Low-temperature chemistry triggered by probe cooling in a low-pressure premixed flame. *Combust Flame*. 2019;204:260-267.
34. Krüger D, Oßwald P, Köhler M, et al. Hydrogen abstraction ratios: a systematic iPEPICO spectroscopic investigation in laminar flames. *Combust Flame*. 2018;191:343-352.
35. Bodi A, Hemberger P, Gerber T, Sztáray B. A new double imaging velocity focusing coincidence experiment: i^{2}PEPICO. *Rev Sci Instrum*. 2012;83:083105.
36. Sztáray B, Voronova K, Torma KG, et al. CRF-PEPICO: double velocity map imaging photoelectron photoion coincidence spectroscopy for reaction kinetics studies. *J Chem Phys*. 2017;147:013944.
37. Hoener M, Kaczmarek D, Bierkandt T, Bodi A, Hemberger P, Kasper T. A pressurized flow reactor combustion experiment interfaced with synchrotron double imaging photoelectron photoion coincidence spectroscopy. *Rev Sci Instrum*. 2020;91:045115.
38. Oßwald P, Hemberger P, Bierkandt T, et al. *In situ* flame chemistry tracing by imaging photoelectron photoion coincidence spectroscopy. *Rev Sci Instrum*. 2014;85:025101.

39. Hansen N, Cool TA, Westmoreland PR, Kohse-Höinghaus K. Recent contributions of flame-sampling molecular-beam mass spectrometry to a fundamental understanding of combustion chemistry. *Prog Energy Combust Sci*. 2009;35:168-191.
40. Egolfopoulos FN, Hansen N, Ju Y, Kohse-Höinghaus K, Law CK, Qi F. Advances and challenges in laminar flame experiments and implications for combustion chemistry. *Prog Energy Combust Sci*. 2014;43:36-67.
41. Li Y, Zhou C-W, Somers KP, Zhang K, Curran HJ. The oxidation of 2-butene: a high pressure ignition delay, kinetic modeling study and reactivity comparison with isobutene and 1-butene. *Proc Combust Inst*. 2017;36:403-411.
42. Metcalfe WK, Burke SM, Ahmed SS, Curran HJ. A hierarchical and comparative kinetic modeling study of C_1−C_2 hydrocarbon and oxygenated Fuels. *Int J Chem Kinet*. 2013;45:638-675.
43. Jithin EV, Dinesh K, Mohammad A, Velamati RK. Laminar burning velocity of *n*-butane/hydrogen/air mixtures at elevated temperatures. *Energy*. 2019;176:410-417.
44. Jiang X, Pan Y, Sun W, Liu Y, Huang Z. Shock-tube study of the autoignition of *n*-butane/hydrogen mixtures. *Energy Fuels*. 2018;32:809-821.
45. Lee S, Song S. A rapid compression machine study of hydrogen effects on the ignition delay times of *n*-butane at low-to-intermediate temperatures. *Fuel*. 2020;266:116895.
46. Chemical Workbench. http://www.kintechlab.com/, Version 4.1.19528, 2017. Accessed June 21, 2020.
47. Moshammer K, Jasper AW, Popolan-Vaida DM, et al. Detection and identification of the keto-hydroperoxide ($HOOCH_2OCHO$) and other intermediates during low-temperature oxidation of dimethyl ether. *J Phys Chem A*. 2015;119:7361-7374.
48. Meloni G, Zou P, Klippenstein SJ, et al. Energy-resolved photoionization of alkylperoxy radicals and the stability of their cations. *J Am Chem Soc*. 2006;128:13559-13567.
49. Covert KJ, Voronova K, Torma KG, Bodi A, Zádor J, Sztáray B. Thermochemistry of the smallest QOOH radical from the roaming fragmentation of energy selected methyl hydroperoxide ions. *Phys Chem Chem Phys*. 2018;20:21085-21094.
50. Voronova K, Ervin KM, Torma KG, et al. Radical thermometers, thermochemistry, and photoelectron spectra: a photoelectron photoion coincidence spectroscopy study of the methyl peroxy radical. *J Phys Chem Lett*. 2018;9:534-539.
51. Curtiss LA, Redfern PC, Raghavachari K. Gaussian-4 theory. *J Chem Phys*. 2007;126:084108.
52. Frisch MJ, Trucks GW, Schlegel HB, et al. *Gaussian 16, Revision A.03*. Wallingford, CT: Gaussian; 2016.
53. Mozhayskiy VA, Krylov AI, *ezSpectrum*. http://iopenshell.usc.edu/downloads. Accessed June 21, 2020.
54. Noell AC, Laboratory studies of the self and cross reactions of atmospheric peroxy radicals. PhD thesis, California Institute of Technology, 2010.
55. Kimura K, Osafune K. Photoelectron spectroscopic study of skew compounds. III. N,N′-Dimethylhydrazine, dimethyl peroxide, and dimethyl disulfide. *Bull Chem Soc Jpn*. 1975;48:2421-2427.
56. Yang B, Wang J, Cool TA, Hansen N, Skeen S, Osborn DL. Absolute photoionization cross-sections of some combustion intermediates. *Int J Mass Spectrom*. 2012;309:118-128.
57. Kimura K, Katsumata S, Achiba Y, Yamazaki T, Iwata S. *Handbook of HeI Photoelectron Spectra of Fundamental Organic Molecules*. Tokyo: Japan Scientific Societies Press; 1981.
58. Biermann HW, Morton TH. Reversible tautomerization of radical cations. Photoionization of 2-methoxyethanol and 3-methoxy-1-propanol. *J Am Chem Soc*. 1983;105:5025-5030.
59. Ashmore FS, Burgess AR. Study of some medium size alcohols and hydroperoxides by photoelectron spectroscopy. *J Chem Soc, Faraday Trans 2*. 1977;73:1247-1261.
60. Batich C, Adam W. The photoelectron spectra of alkylperoxides. *Tetrahedron Lett*. 1974;15:1467-1470.
61. Lang M, Holzmeier F, Hemberger P, Fischer I. Threshold photoelectron spectra of combustion relevant C_4H_5 and C_4H_7 isomers. *J Phys Chem A*. 2015;119:3995-4000.
62. Linstrom PJ, Mallard WG, Eds. *NIST Chemistry WebBook*. NIST Standard Reference Database Number 69. Gaithersburg MD: NIST. https://doi.org/10.18434/T4D303. Accessed June 21, 2020.
63. Cool TA, Nakajima K, Mostefaoui TA, et al. Selective detection of isomers with photoionization mass spectrometry for studies of hydrocarbon flame chemistry. *J Chem Phys*. 2003;119:8356-8365.
64. Kasper T, Lucassen A, Jasper AW, et al. Identification of tetrahydrofuran reaction pathways in premixed flames. *Z Phys Chem*. 2011;225:1237-1270.
65. Cool TA, McIlroy A, Qi F, et al. Photoionization mass spectrometer for studies of flame chemistry with a synchrotron light source. *Rev Sci Instrum*. 2005;76:094102.
66. Cool TA, Wang J, Nakajima K, Taatjes CA, McIlroy A. Photoionization cross sections for reaction intermediates in hydrocarbon combustion. *Int J Mass Spectrom*. 2005;247:18-27.
67. Wang J, Yang B, Cool TA, Hansen N, Kasper T. Near-threshold absolute photoionization cross-sections of some reaction intermediates in combustion. *Int J Mass Spectrom*. 2008;269:210-220.
68. Kercher JP, Fogleman EA, Koizumi H, Sztáray B, Baer T. Heats of formation of the propionyl ion and radical and 2,3-pentanedione by threshold photoelectron photoion coincidence spectroscopy. *J Phys Chem A*. 2005;109:939-946.
69. Dampc M, Mielewska B, Siggel-King MRF, King GC, Zubek M. Threshold photoelectron spectra of tetrahydrofuran over the energy range 9–29 eV. *Chem Phys*. 2009;359:77-81.
70. Fogleman EA, Koizumi H, Kercher JP, Sztáray B, Baer T. Heats of formation of the acetyl radical and ion obtained by threshold photoelectron photoion coincidence. *J Phys Chem A*. 2004;108:5288-5294.
71. Xie M, Zhou Z, Wang Z, Chen D, Qi F. Determination of absolute photoionization cross-sections of oxygenated hydrocarbons. *Int J Mass Spectrom*. 2010;293:28-33.
72. Moshammer K, Jasper AW, Popolan-Vaida DM, et al. Quantification of the keto-hydroperoxide ($HOOCH_2OCHO$) and other elusive intermediates during low-temperature oxidation of dimethyl ether. *J Phys Chem A*. 2016;120:7890-7901.
73. Togbé C, Mzé-Ahmed A, Dagaut P. Kinetics of oxidation of 2-butanol and isobutanol in a jet-stirred reactor: experimental study and modeling investigation. *Energy Fuels*. 2010;24:5244-5256.
74. Sun W, Wang J, Huang C, Hansen N, Yang B. Providing effective constraints for developing ketene combustion mechanisms: a detailed kinetic investigation of diacetyl flames. *Combust Flame*. 2019;205:11-21.

75. Stepowski D, Puechberty D, Cottereau MJ. Use of laser-induced fluorescence of OH to study the perturbation of a flame by a probe. *Symp (Int) Combust*. 1981;18:1567-1573.
76. Biordi JC, Lazzara CP, Papp JF. Molecular beam mass spectrometry applied to determining the kinetics of reactions in flames. I. Empirical characterization of flame perturbation by molecular beam sampling probes. *Combust Flame*. 1974;23:73-82.
77. Desgroux P, Gasnot L, Pauwels JF, Sochet LR. Correction of LIF temperature measurements for laser absorption and fluorescence trapping in a flame. *Appl Phys B*. 1995;61:401-407.
78. Struckmeier U, Oßwald P, Kasper T, et al. Sampling probe influences on temperature and species concentrations in molecular beam mass spectroscopic investigations of flat premixed low-pressure flames. *Z Phys Chem*. 2009;223:503-537.
79. Gururajan V, Egolfopoulos FN, Kohse-Höinghaus K. Direct numerical simulations of probe effects in low-pressure flame sampling. *Proc Combust Inst*. 2015;35:821-829.
80. Deng L, Kempf A, Hasemann O, Korobeinichev OP, Wlokas I. Investigation of the sampling nozzle effect on laminar flat flames. *Combust Flame*. 2015;162:1737-1747.
81. Hansen N, Tranter RS, Moshammer K, et al. 2D-imaging of sampling-probe perturbations in laminar premixed flames using Kr X-ray fluorescence. *Combust Flame*. 2017;181:214-224.
82. Karakaya Y, Sellmann J, Wlokas I, Kasper T. Influence of the sampling probe on flame temperature, species, residence times and on the interpretation of ion signals of methane/oxygen flames in molecular beam mass spectrometry measurements. *Combust Flame*. 2021;229:111388.

SUPPORTING INFORMATION

Additional supporting information may be found online in the Supporting Information section at the end of the article.

How to cite this article: Bierkandt T, Oßwald P, Gaiser N, et al. Observation of low-temperature chemistry products in laminar premixed low-pressure flames by molecular-beam mass spectrometry. *Int J Chem Kinet*. 2021;53:1063–1081. https://doi.org/10.1002/kin.21503